Polycrystalline Methane Hydrate: Synthesis from Superheated Ice, and Low-Temperature Mechanical Properties

Laura A. Stern* and Stephen H. Kirby†

Western Earthquake Hazards Team, U.S. Geological Survey, MS/977, 345 Middlefield Road, Menlo Park, California 94025

William B. Durham‡

Lawrence Livermore Laboratory, Livermore, California 94550

Received September 8, 1997. Revised Manuscript Received November 17, 1997

We describe a new and efficient technique to grow aggregates of pure methane hydrate in quantities suitable for physical and material properties testing. Test specimens were grown under static conditions by combining cold, pressurized CH_4 gas with granulated H_2O ice, and then warming the reactants to promote the reaction $CH_4(g) + 6H_2O(s \rightarrow l) \rightarrow CH_4 \cdot 6H_2O$ (methane hydrate). Hydrate formation evidently occurs at the nascent ice/liquid water interface on ice grain surfaces, and complete reaction was achieved by warming the system above the ice melting point and up to 290 K, at 25−30 MPa, for approximately 8 h. The resulting material is pure, cohesive, polycrystalline methane hydrate with controlled grain size and random orientation. Synthesis conditions placed the H_2O ice well above its melting temperature while reaction progressed, yet samples and run records showed no evidence for bulk melting of the unreacted portions of ice grains. Control experiments using Ne, a non-hydrate-forming gas, showed that under otherwise identical conditions, the pressure reduction and latent heat associated with ice melting are easily detectable in our fabrication apparatus. These results suggest that under hydrate-forming conditions, H_2O ice can persist metastably to temperatures well above its ordinary melting point while reacting to form hydrate. Direct observations of the hydrate growth process in a small, high-pressure optical cell verified these conclusions and revealed additional details of the hydrate growth process. Methane hydrate samples were then tested in constant-strain-rate deformation experiments at $T = 140-200$ K, $P_c = 50-100$ MPa, and $\dot{\epsilon} = 10^{-4}-10^{-6}$ s^{-1}. Measurements in both the brittle and ductile fields showed that methane hydrate has measurably different strength than H_2O ice, and work hardens to an unusually high degree compared to other ices as well as to most metals and ceramics at high homologous temperatures. This work hardening may be related to a changing stoichiometry under pressure during plastic deformation; X-ray analyses showed that methane hydrate undergoes a process of solid-state disproportionation or exsolution during deformation at conditions well within its conventional stability field.

Introduction

Methane hydrate is a nonstoichiometric compound consisting of a network of H_2O molecules that are hydrogen-bonded in a manner similar to ice and interstitially encaging CH_4 gas molecules.[1] Distributed globally in shallow marine and permafrost environments, methane hydrate harbors a significant yet virtually untapped hydrocarbon source.[2−4] Despite scientific interest in this compound and potential commercial importance, many of the physical, chemical, and material properties of methane hydrate are as yet poorly constrained or unmeasured, and a full understanding of these properties will eventually be needed to turn potential energy projections into practical plans for its recovery. We have now established optimal growth parameters for efficient synthesis of methane hydrate suitable for such testing and have determined the fracture and flow characteristics of these samples in

* Corresponding author. Tel: (650) 329-4811. Fax: (650) 329-5163. Email: lstern@isdmnl.wr.usgs.gov.

† Tel: (650) 329-4847. Fax: (650) 329-5163. Email: skirby@isdmnl.wr.usgs.gov.

‡ U. C. Lawrence Livermore National Laboratory, P.O. Box 808, Livermore, CA 94550. Tel: (510) 422-7046. Fax: (510) 423-1057. Email: durham1@llnl.gov.

(1) Natural gas hydrates belong to either of two crystal structures; methane hydrate ($CH_4 \cdot 5.75H_2O$, ideally) is a structure I hydrate (1.2 nm cubic unit cell, space group *Pm*3*n*), constructed from 46 H_2O molecules and 8 cavities available for CH_4 gas molecules.

(2) Sloan, E. *Clathrate Hydrates of Natural Gases*; Marcel Dekker, Inc.: New York, 1990; p 641.

(3) Kvenvolden, K. *Chem. Geol.* **1988**, *71*, 41−51.

(4) Because methane hydrate concentrates CH_4 by a factor of about 170 with respect to STP gas and as little as 10% of the recovered energy is required for dissociation, hydrate reservoirs are considered a substantial future energy resource; it has been estimated that the total amount of gas in this solid form may surpass the energy content of the total fossil fuel reserves by as much as a factor of 2 (refs 2, 3, and also: Claypool, G. E.; Kaplan, I. R. In *Natural Gases in Marine Sediments*; Kaplan, I. R., Ed.; Plenum Press: New York, 1974; pp 99−139.

S0887-0624(97)00167-9 CCC: $15.00
Published on Web 01/23/1998

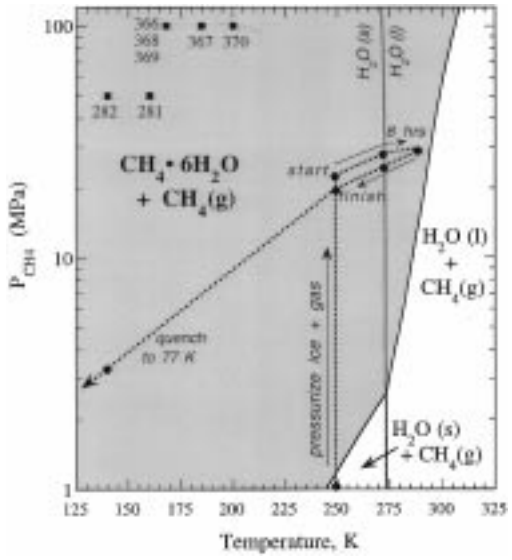

Figure 1. Phase diagram for the CH_4-H_2O system. Shaded region shows field of methane hydrate stability. At low pressures or high temperatures, methane hydrate dissociates to H_2O (ice or liquid) plus CH_4 gas. The metastable extension of the H_2O melting curve is shown by the gray curve. Dashed lines trace the reaction path during sample synthesis (described in text). Solid squares show P and T conditions of deformation tests.

deformation experiments. The results revealed a number of anomalous aspects of the formation, stability, and plastic flow behavior of methane hydrate at elevated pressure.[5]

Sample Synthesis

Our objectives were to (1) synthesize large-volume, cohesive, polycrystalline hydrate aggregates with full methane saturation, uniform grain size, and random crystallographic grain orientation, and (2) develop optimal synthesis parameters to produce such test specimens efficiently. The technique that we developed differs significantly from previous studies,[6] many of which involve continuous agitation of reaction mixtures at low to moderate pressures, resulting in strongly textured material and/or containing low methane content or significant fractions of ice (or water), and therefore unsuitable for materials testing. We produced samples of pure methane hydrate by the general reaction $CH_4(g) + 6H_2O(s \rightarrow l) \rightarrow CH_4 \cdot 6H_2O(s)$ (Figure 1), by the mixing and subsequent slow, regulated heating of sieved granular ice ("seed" ice) and cold, pressurized CH_4 gas in an approximately constant-volume reaction vessel (Figures 2 and 3). This "seeding" method for hydrate nucleation and growth was developed from our previous studies of H_2O-based icy compounds,[7] in which we demonstrated successful growth of polycrystalline test specimens with controlled and uniform grain size with no preferred crystallographic orientation. Such sample characteristics, devoid of grain size or anisotropy effects, are necessary for reliable characterization of the intrinsic mechanical behavior of crystalline solids.

Sample fabrication details are as follows: CH_4 gas from a source bottle is initially boosted in pressure (P) by a gas intensifier and routed into sample molding vessels housed in a deep freezer. The sample assembly, shown in Figure 2, is an upgraded design from that described previously,[5] and consists of three steel vessels immersed in an ethyl alcohol bath initially held at freezer temperature (T) of 250 K. One vessel serves as a reservoir to store and chill pressurized CH_4 gas, and the others house the sample molds (two samples can be fabricated concurrently, or the valve to the second sample chamber can be closed off in order to make only a single sample.) Each sample mold consists of a hollow split cylinder that encases an indium sleeve filled with 26 g of H_2O ice seed grains, packed to ~40% porosity. Seed material is made from a gas-free, single-crystal block of ice grown from triply distilled H_2O, ground and sieved to 180−250 μm grain size. Initially, the sample chambers with seed ice are closed off from the reservoir and are evacuated. A loosely fitting top disk inserted on top of the packed seed ice grains (Figures 2 and 3) prevents displacement of the packed ice grains during evacuation.

The reservoir vessel is first charged with pressurized CH_4 gas to 35 MPa and cools to 250 K. When fabricating a single sample, the reservoir is opened to the preevacuated sample chamber and CH_4 pressure (P_{CH_4}) drops to roughly 23 MPa. During fabrication of double samples, the reservoir charging, cooling, and opening procedure is repeated to bring the larger volume of the two-sample system to 23 MPa at 250 K. These steps serve to fill the porosity between the ice grains at a molar ratio of CH_4 to H_2O in the sample vessels well in excess of that required for full hydrate formation.[8−10] The bath temperature is then slowly raised by means of the hot plate situated beneath the alcohol bath (Figure 2). As the samples and reservoir contents warm, they self-pressurize. Pressure increases steadily with increasing temperature until reaction initiates, at which point consumption of CH_4 gas by hydrate formation slows the rate of pressure increase (Figure 4). Data-acquisition software (LabVIEW, National Instruments) was used to monitor and record pressure and temperature conditions throughout each run, and the extent of reaction was determined by the measured P_{CH_4} offset from the reversible CH_4 expansion curve.

Following full reaction, the heat source is turned off, the system slowly cools back down to 250 K, and the sample chambers are isolated from the reservoir. The samples are then vented while quenched in liquid nitrogen, disconnected from the apparatus, and opened.

(5) Stern, L.; Kirby, S.; Durham, W. *Science* **1996**, *273*, 1843−1848.

(6) Barrer, R.; Ruzicka, D. *Trans. Faraday Soc.* **1962**, *58*, 2253. Barrer, R.; Edge, A. *Proc. R. Soc. (London)* **1967**, *A300*, 1. Falabella, B.; Vanpee, M. *Ind. Eng. Chem. Fundam.* **1974**, *13*, 228. Aoyogi, K.; Song, K.; Kobayashi, R.; Sloan, E.; Dharmawardhana, P. Gas Processors Assn. Research Report No. 45, Tulsa, OK, 1980. See Sloan[2] for full review of fabrication techniques.

(7) Durham, W.; Heard, H.; Kirby, S. *Proc. Lunar Planet. Sci. Conf. 14th*, part 1; *J. Geophys. Res.* **1983**, *88*, Suppl. B377−B392, 433−441. Durham, W.; Kirby, S.; Stern, L. *J. Geophys. Res.* **1992**, *97* (E12), 20883−20897. Durham, W.; Kirby, S.; Stern, L. *J. Geophys. Res.* **1993**, *98* (B10), 17667−17682.

(8) Makogan[9] first suggested that as hydrate formation is an interfacial process, high concentrations of hydrate-forming species are required at the interface. Hwang *et al.*[10] confirmed that a high-pressure driving force is required for measurable hydrate formation rates, and that for hydrate formation from melting ice, higher gas pressure yields higher formation rates.

(9) Makogan, Y. *Hydrates of Natural Gases*; Cielewicz, W. H., Translator; PennWell: Tulsa, OK, 1981.

(10) Hwang, M. J.; Wright, D. A.; Kapur, A.; Holder, G. D. *J. Inclusion Phenom.* **1990**, *8*, 103−116.

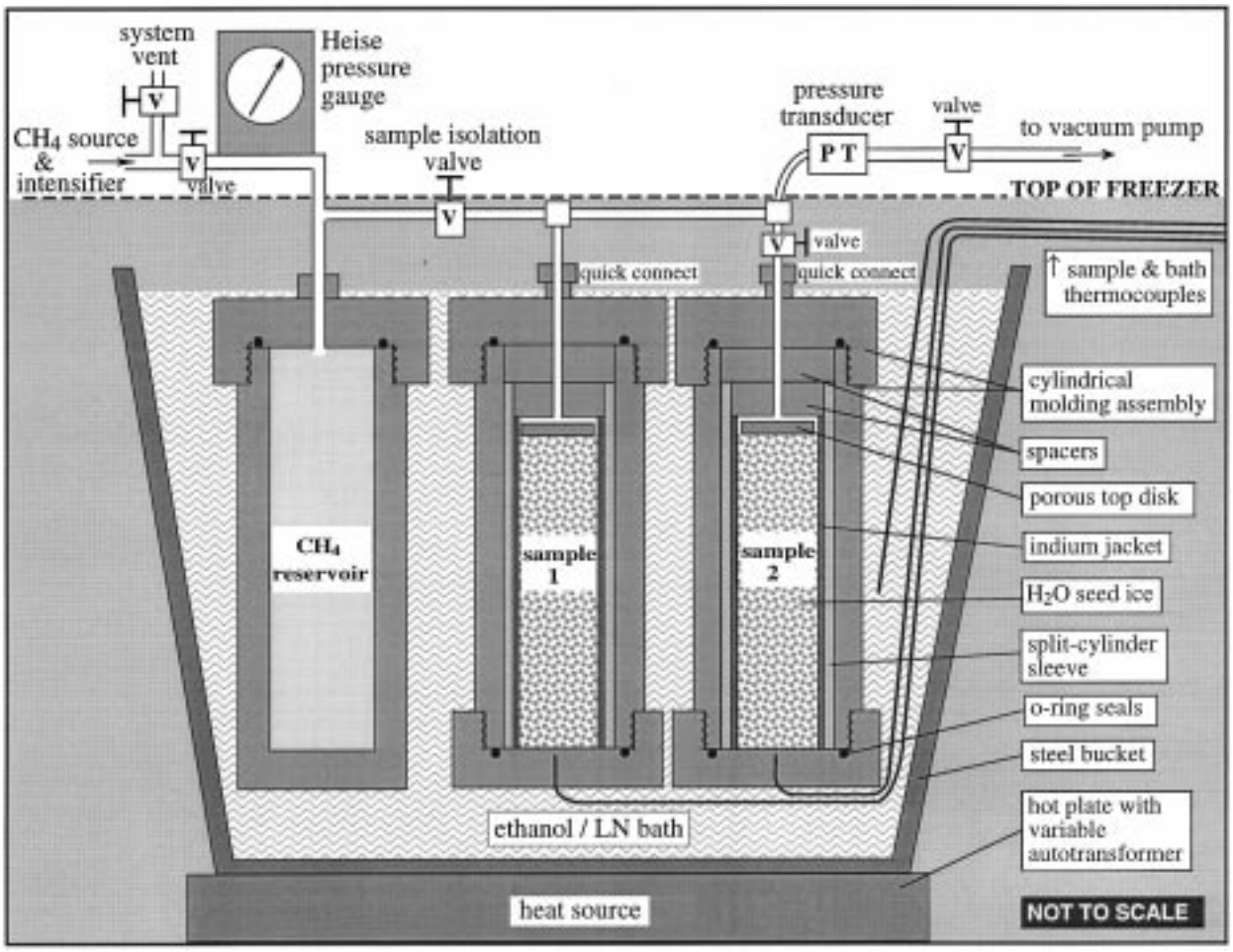

Figure 2. Apparatus for fabricating cylindrical test specimens of methane hydrate from CH_4 gas and H_2O ice. The sample assembly is housed in a freezer at 250 K, and consists of three steel vessels immersed in an ethyl alcohol bath. One vessel stores a reservoir of cold, pressurized CH_4 gas at 35 MPa and 250 K, and the others contain sample molds with prejacketed and preevacuated H_2O seed ice. Two-way valves allow isolation of any component of the assembly, and a vacuum pump connected to the sample chambers permits evacuation of the system. The sample chambers are warmed by a hot plate situated beneath the alcohol bath and controlled remotely with a variable autotransformer. Temperature is monitored by thermocouples emplaced in the base of the sample mold and in the bath, and pressure is measured by the gauge and transducer, as shown. Procedures promoting methane hydrate synthesis are described in the text.

The inner, hollow split-cylinders containing the jacketed samples are pushed from the molds and pried off the samples. The jacketed samples are then stored in or directly above liquid nitrogen prior to mechanical testing.

The Hydrate-Forming Reaction

***P*−*T*−*t* Relations.** Representative pressure−temperature (*P*−*T*) and temperature−time (*T*−*t*) histories during complete reaction of a single-sample run are shown in Figure 4. Up to 271.5 K, P_{CH_4} increases approximately linearly with temperature with a slope governed primarily by the equilibrium thermal expansion of free CH_4 in the reservoir and sample reaction vessel. Progress of the hydrate-forming reaction was monitored by observing the deflection of *P* from this linear *P*−*T* curve, a deflection that accompanies the volume reduction associated with reaction. Completion of reaction is marked by a *P* offset (ΔP_r) of 1.8 ± 0.1 MPa at a peak temperature of ∼289 ± 1 K, a state that is reached over a heating time interval of about 8 h after the sample vessel crosses the 271.5 K isotherm (Figure 4). After cooling to 77 K while venting excess CH_4, the resulting samples were shown by X-ray diffraction measurements to be virtually pure methane hydrate, with minor amounts of ice (0−3%) being the only additional phase (Figure 5A). That essentially all the H_2O reacted to form hydrate was also consistent with both the calculated molar volume reduction of the reaction,[11] and with the lack of a *P*−*T* anomaly associated with freezing of unreacted liquid water (Figure 4A, cooling curve). Measurements of the mass uptake of CH_4 in fully reacted samples also were consistent with complete reaction of the original H_2O to form hydrate of composition near $CH_4 \cdot 6.1H_2O$ (±0.1H_2O), which is the expected equilibrium stoichiometry for this compound

(11) The volume of an empty structure I hydrate lattice is 16% greater than the equivalent mass of ice I [the empty structure I lattice has a density of 0.78, and stoichiometric methane hydrate has a density near ice (0.90 vs 0.92 for ice)], but there is a large $-\Delta V$ associated with hydrate formation due to the volume reduction of the gas phase into the hydrate structure. Here, when fabricating a single sample, we start with 26 g of seed ice and the actual molar reaction is: $1.4H_2O + 0.23\ CH_4(g) \rightarrow 0.23(CH_4 \cdot 6.1H_2O)$. The 3.8 g of CH_4 uptake measured in each sample after synthesis confirms this hydrate stoichiometry and is consistent with ref 12. While ΔV of the reaction is nearly 21%, we measure only a 6.4% associated drop from the starting *P* due to the large volume of the combined reservoir plus sample chamber.

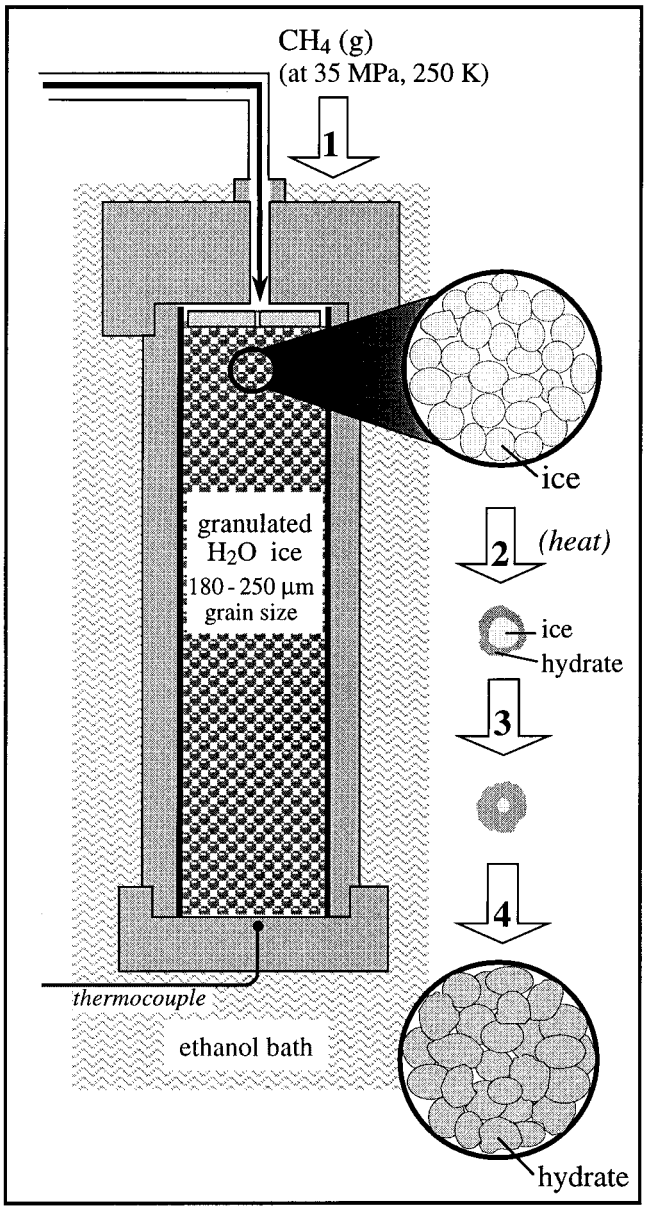

Figure 3. Schematic diagram illustrating our postulated model for hydrate synthesis from H_2O ice plus CH_4 gas, by the methods described in the text. Numbered arrows (1−4) are as follows: (1) Cold, pressurized CH_4 gas (35 MPa, 250 K) is admitted to preevacuated, fine-grained, H_2O seed ice in the sample chamber. The reactants equilibrate to ~23 MPa and 250 K. (2) Warming the reactants above the H_2O melting point (271.5 K at 25 MPa) initiates measurable hydrate formation at the surface of the ice grains, creating composite grains in which a mantle of hydrate envelops an unreacted ice core. The reaction rate (diffusion controlled) slows as the hydrate rind grows and thickens (see text). (3) Slowly raising the temperature to ~290 K over 8 h promotes full reaction, yet no evidence for bulk melting of the H_2O ice was observed (see Figures 4 and 6). (4) Near the end of the heating cycle, all the ice reacts to form hydrate.

at approximately 25−30 MPa methane pressure.[11−13] The resulting samples are translucent, white, cohesive

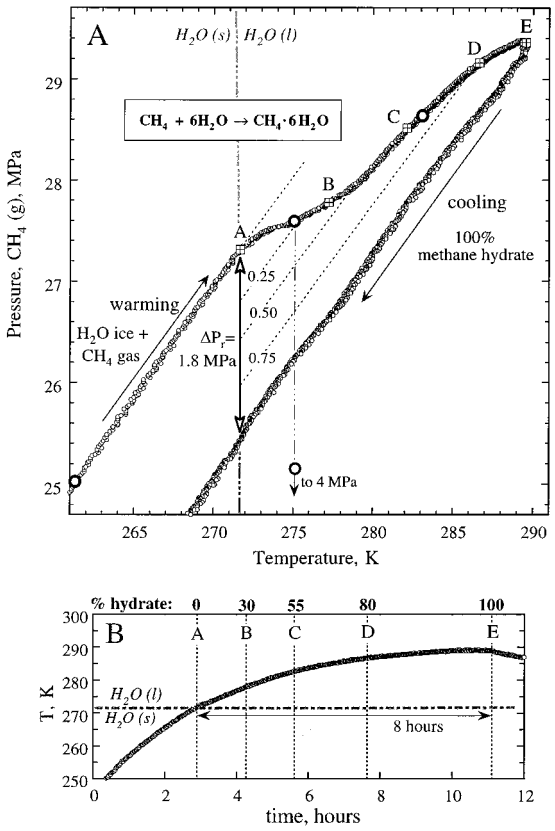

Figure 4. (A) Temperature−pressure *(T−P)* history of a typical methane hydrate synthesis run (single sample) promoting the hydrate-forming reaction: $CH_4(g) + H_2O(ice) \rightarrow CH_4{\cdot}6H_2O$. Warming the ice + gas mixture above the H_2O solidus (dot−dashed line; square A) initiates macroscopic reaction. Increasing temperature slowly to 290 K, over an 8 h span, promotes full reaction. Complete reaction in our apparatus is marked by a 1.8 MPa pressure drop (ΔP_r) from start to finish relative to the extrapolated subsolidus $P-T$ curve. Squares A−E correspond to peak $P-T$ conditions of individual samples that were quenched at specific intervals during hydrate formation to determine hydrate content as a function of ΔP_r and time. Open circles designate the $P-T$ conditions corresponding to the optical cell photographs shown in Figure 7. (B) Temperature-time profile during hydrate formation. Hydrate content (vol %) of samples A−E is given on the top scale bar and shows how the rate of hydrate formation decays with time under static growth conditions.

aggregates of uniformly fine, equant grains with 250 ± 50 μm grain size. Samples, as molded, contain 29 ± 1% porosity after full reaction,[11] and this porosity is eliminated by externally pressurizing sealed samples while venting the pore space gas, as discussed later.

Hydrate Formation from Superheated Ice. The detailed $P-T-t$ curves (Figure 4) and analyses of recovered samples revealed unexpected aspects of the reaction process. Figure 4A shows that deviation of the $P-T$ record from the CH_4 self-pressurization curve first occurs just above the expected melting temperature of H_2O ice, 271.5 K at 28 MPa. As time proceeds, the rate of P_{CH_4} increase slows as the hydrate-forming reaction consumes CH_4 gas. Lack of appreciable reaction of CH_4 with ice below the H_2O liquidus was expected, in light of earlier investigations.[6,10]

After approximately $0.5\Delta P_r$ (Figure 4A), the reaction rate decreased markedly. Full reaction was most efficiently achieved by continuing to warm the system to conditions approaching the methane hydrate dissocia-

(12) Gas hydrate number n varies with P; increasing P maximizes guest-molecule site occupancy. At sample synthesis conditions (~28 MPa) n for methane hydrate should be 6.1 ± 0.1, and at 100 MPa n = 5.85 ± 0.05 (Saito, S.; Marshall, D.; Kobayashi, R. *AIChE J.* **1964**, *10*, 734. Also see ref 13, p 54.)

(13) *Handbook of gas hydrate properties and occurrence.* U.S. DOE Publication DOE/MC/19239-1546, 1983; 234 pages.

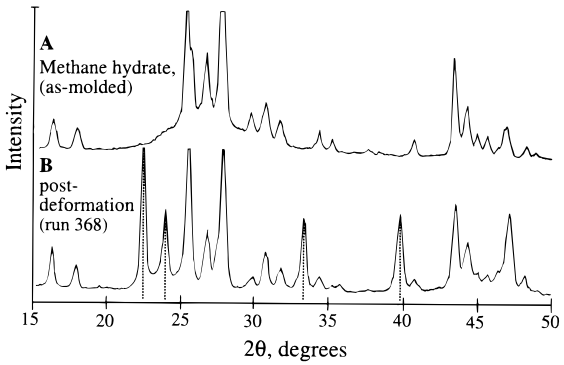

Figure 5. X-ray powder diffraction patterns for methane hydrate, as-grown (A), and after mechanical testing (B). Methane hydrate deformed under nonhydrostatic stress apparently undergoes a partial solid-state disproportionation (see text), as evidenced by H_2O ice peaks (dotted lines) found in postdeformation X-ray diffraction patterns.

tion curve and well above the metastable extension of the H_2O melting curve (Figures 1 and 4). To determine the rate of conversion of ice to hydrate at these optimal conditions of T and P as a function of time, a series of partial-reaction experiments were quenched at various points along the full reaction curve, and subsequently weighed and X-rayed to determine methane hydrate content (Figure 4, squares A−E). These partial-reaction tests indicated that during the early stages of reaction up to values of roughly $0.4\Delta P_r$, the slow rate of seed ice melting still slightly exceeded hydrate formation, as there was less methane hydrate in the samples than would be predicted by ΔP_r (Figure 4B, top scale bar; see ref 5 for further discussion). After this period, the rate of hydrate formation essentially kept pace with incipient melting for the remainder of the 8 h needed for full reaction at these conditions.

Figure 4 shows that there are no $P-T$ discontinuities in the run records to indicate bulk melting of the seed ice in the sample mold, even though full reaction to form methane hydrate at these conditions requires about 8 h at temperatures well above the H_2O melting curve. The positive slope of the $P-T$ curve within a few degrees above 271.5 K shows that there is not immediate and full melting of the ice as it is warmed above its liquidus, and there is a period of several tens of minutes after crossing the liquidus before there is any substantial indication of either ice melting or hydrate forming. These observations point to the conclusion that much of the seed ice exists in a superheated state for the many hours needed for full methane hydrate conversion.

This conclusion was verified by control experiments using neon (Ne, a non-hydrate-forming gas) in place of CH_4 gas, under the same environmental conditions and in the same apparatus as the methane hydrate samples (Figure 6). We have previously described these results[5] and briefly outline them here. The Ne experiments confirmed that rapid and complete melting of the H_2O ice during the heating phase and refreezing of ice during the cooling phase of the tests occurs in our apparatus when ice is not in the presence of a hydrate-forming gas, and that the associated $P-T$ anomalies are easily detected (Figure 6A, bottom curve). Moreover, the temperature measured by the Ne sample thermocouple lagged the rising temperature in the surrounding alcohol bath during the time interval over which the

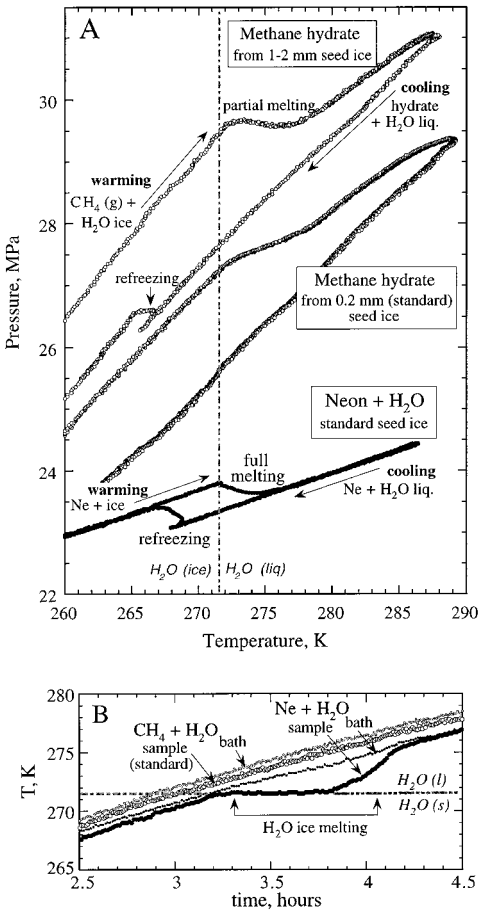

Figure 6. (A) Temperature−pressure ($T-P$) records of methane hydrate fabrication runs made from coarse-grained seed ice (top curve) and fine-grained, "standard" seed ice (middle curve, also shown in Figure 4) compared to a neon gas (Ne) + H_2O ice experiment (bottom curve). The Ne + H_2O ice experiment demonstrates full melting and refreezing of all H_2O seed ice near its solidus (gray dot−dashed line) when in the presence of non-hydrate-forming gas. The Ne + ice run shows no net P drop associated with melting and refreezing, so that start−finish conditions are coincident. Methane hydrate formation by our standard procedures (middle curve) shows no evidence for melting of the seed ice, or refreezing of H_2O melt during cooling, and produces samples of pure, granular methane hydrate with uniform grain size. In contrast, fabrication runs using coarse-grained seed ice (1−2 mm) were unsuccessful in producing efficient synthesis of pure hydrate and showed both textural and run record evidence for substantial melting of the seed ice. Coarse-grained samples that were maintained at peak conditions for durations between 8 and 25 h all contained significant fractions of liquid H_2O that did not form hydrate and that produced large $P-T$ discontinuities upon refreezing (top curve, cooling trend). (B) Detail of the temperature−time profile of Ne + H_2O ice in the region of ice melting, showing the lag of the sample temperature compared to the bath temperature associated with the absorption of heat by the endothermic melting of ice. No such effect is displayed by the thermal history of a standard methane hydrate experiment, also shown.

pressure dropped (Figure 6B), a phenomenon that we attribute to the absorption of heat by the expected endothermic melting of ice. In comparison, the temperature records of standard CH_4 runs (Figure 6, middle curve; also Figure 4) displayed no such thermal anomalies, indicating that rapid, wholesale melting did not occur.[14] A prominent refreezing $P-T$ anomaly occurred during the cooling phase of the Ne runs, and no P offset

was detected after returning to the starting temperature. Visual inspection and X-ray identification of the final, quenched samples from the Ne experiments showed that they consisted of clear cylinders of H_2O ice in the bottom of the mold and that the loosely fitting top disk had sunk to the bottom, indicating full melting. In contrast, fully reacted methane hydrate samples have uniformly fine-grained granular textures and no displacement of the top disk occurs. The neon control experiments thus demonstrated that all the indicators of ice melting expected in our apparatus are actually observed when a non-hydrate-forming gas is used in the place of methane. The lack of such indicators in the methane experiments implies that such melting does not occur when hydrate forms during our standard fabrication procedures.

Grain-Size Effects. Tests in which we used a coarser-sized seed ice fraction (1−2 mm) showed evidence for significant melt accumulation in the sample chamber during the heating cycle (Figure 6A, compare top and middle curves), and were unsuccessful in producing bulk, granular aggregates of pure methane hydrate. Unlike the standard methane hydrate $P-T$ records, those from the coarse-grained samples showed measurable pressure discontinuities associated with melting during the warming phase of synthesis. Even those samples that were maintained at peak $P-T$ conditions for over 25 h did not fully react; these samples showed large H_2O freezing signatures in their $P-T$ cooling curves and contained large fractions of ice upon recovery, likely due to the known difficulty in nucleating and forming methane hydrate from a bulk liquid (similar to bulk ice) under static conditions.[15] The final, recovered samples also displayed markedly different textures than those from fine-grained (standard) ice; the coarse-grained samples had icy and pluglike textures where the accumulated liquid descended into the bottom half of the mold to partially fill the available pore space.

Direct Observation of Hydrate Formation. We further investigated the process of methane hydrate formation by direct observation, using a small, high-pressure optical cell[16] in which we duplicated our sample fabrication procedures while observing the reaction under a microscope.[17] For these tests, we initially chilled the cell and loosely filled it with 200 μm ice grains prepared identically to those used in our large-volume samples. The remaining pore volume was evacuated and then flooded with cold CH_4 gas at 23 MPa and 255 K. Similar tests were also conducted using CO_2 as the hydrate-forming species, in which case the cell was loaded with 6 MPa of CO_2 after being filled with seed ice and evacuated. The cell was then immersed in an insulated dish of cold ethanol, placed under a microscope, and then slowly warmed from 255 to 290 K (when testing CH_4) or to 282 K (for CO_2)[18] at a rate similar to that used during our standard fabrication procedures (Figure 4B).

Ice grains were repeatedly subjected to both CH_4 and CO_2 hydrate forming conditions, and we observed the superheating effect in both environments. Hydrate-plated ice grains persisted to 290 K at 30 MPa in CH_4 (Figure 7) and to 282 K at 8 MPa in CO_2. At temperatures well below the H_2O liquidus, visible surface reaction on the ice grains occurred after relatively brief exposure (<5 min) to either of these species[19] (Figure 7A). Under CH_4 hydrate forming conditions, this initial surface appearance did not change appreciably until the grains were subsequently warmed through the H_2O liquidus (271.5 K at $P_{CH_4} = 27$ MPa). Upon further heating, no expulsion of water was observed nor any cracking or collapsing of the hydrate encasement that should attend bulk melting of the ice interiors, particularly within the first 30 min above the H_2O liquidus when the hydrate rinds are thin and presumably weak. Instead, all grains maintained identifiable shapes and sizes throughout reaction[20] (Figure 7, B and C) and changed only by becoming increasingly mottled in appearance as they approached full conversion to hydrate (see ref 17 for further discussion).

In a separate experimental sequence, melting of interior, unreacted ice within partially-reacted grains was successfully induced at temperatures above the H_2O liquidus, with no attendant dissociation of the outer hydrate mantle. In this experiment, ice grains were first mixed with CH_4 at 23 MPa and then slowly warmed from 255 to 276 K. After 0.75 h above the H_2O liquidus, P_{CH_4} was reduced to 4 MPa, close to dissociation conditions, but still within the methane hydrate stability field (Figures 1 and 4).

Bulk melting of ice in the grain interiors was readily apparent within 10 min of reducing P_{CH_4}. Interior melting produced progressively misshapen grains that

(14) The reaction $CH_4(g) + 6H_2O(ice) \rightarrow CH_4 \cdot 6H_2O$ liberates a small amount of latent heat [$\approx 20 \pm 0.3$ kJ/mol at 273 K and 28 MPa P_{CH_4}, determined from the Clapeyron slope (Makogon, T.; Sloan, E. *J. Chem. Eng. Data* **1994**, *39*, 351−353), the measured enthalpy of formation at standard conditions (Handa, Y. *Chem Thermodyn.* **1986**, *18*, 915−921), ΔV,[11] and its variation with P[12,13]]. This heat is not reflected as a temperature anomaly (Figure 6B), evidently because reaction occurs over a period of 8 h and such heat would be small compared with the exchange of heat of the sample with its surroundings by thermal conduction. (The standard enthalpy for melting of ice is −6.01 kJ/mol, or −36 kJ/ 6 mol H_2O for comparison with the hydrate-forming reaction).

(15) The importance of vigorous agitation to renew ice and/or water surfaces for hydrate formation was established by Villard (Villard, P. *Compt. Rend.* **1888**, *106*, 1602) and is also discussed by Sloan[2] and Hwang et al.[10]

(16) Chou, I.; Pasteris, J.; Seitz, J. *Geochim. Cosmochim. Acta* **1990**, *54*, 535.

(17) Stern, L.; Hogenboom, D.; Durham, W.; Kirby, S.; Chou, I−M. Optical cell evidence for superheated ice under gas-hydrate-forming conditions, *J. Phys. Chem. B.*, in press.

(18) During CO_2 hydrate formation, persistence of partially-reacted ice grains to temperatures above the H_2O liquidus was observed when using either liquid or gaseous CO_2 as the hydrate-forming species. Most tests were conducted using liquid CO_2 in order to trace the superheating effect to higher temperatures before dissociation conditions were reached. The equilibrium formation of CO_2 hydrate occurs at considerably lower $P-T$ conditions than CH_4 hydrate, and its dissociation curve becomes strongly temperature-dependent at $P > 4.5$ MPa where it intersects the CO_2 vapor curve at a corresponding dissociation temperature of 283 K [see Figure 9 in: Ross, R.; Kargel, J. In *Solar System Ices*; Schmitt, B., de Bergh, C., Festou, M., Eds.; Kluwer Academic: Dordrecht, in press); also: Takenouchi, S.; Kennedy, G. *J. Geol.* **1965**, *73*, 383].

(19) We verified that the mottled surface appearance of the grains in the ice subsolidus region (Figure 7A) is caused largely by hydrate formation, rather than ice sublimation, by quickly dropping the P of a sample during the initial stage of reaction and observing partial dissociation of this early-forming hydrate rind.

(20) Observed hydrate formation along the inner wall of the optical cell at temperatures above the H_2O liquidus indicates that H_2O vapor exists in the pore volume of the tube, most likely due to partial sublimation of the hydrate mantle encasing each ice grain. This sublimation process may also explain in part why a significant grain size increase during ice conversion to hydrate is not observed (see also refs 11 and 25).

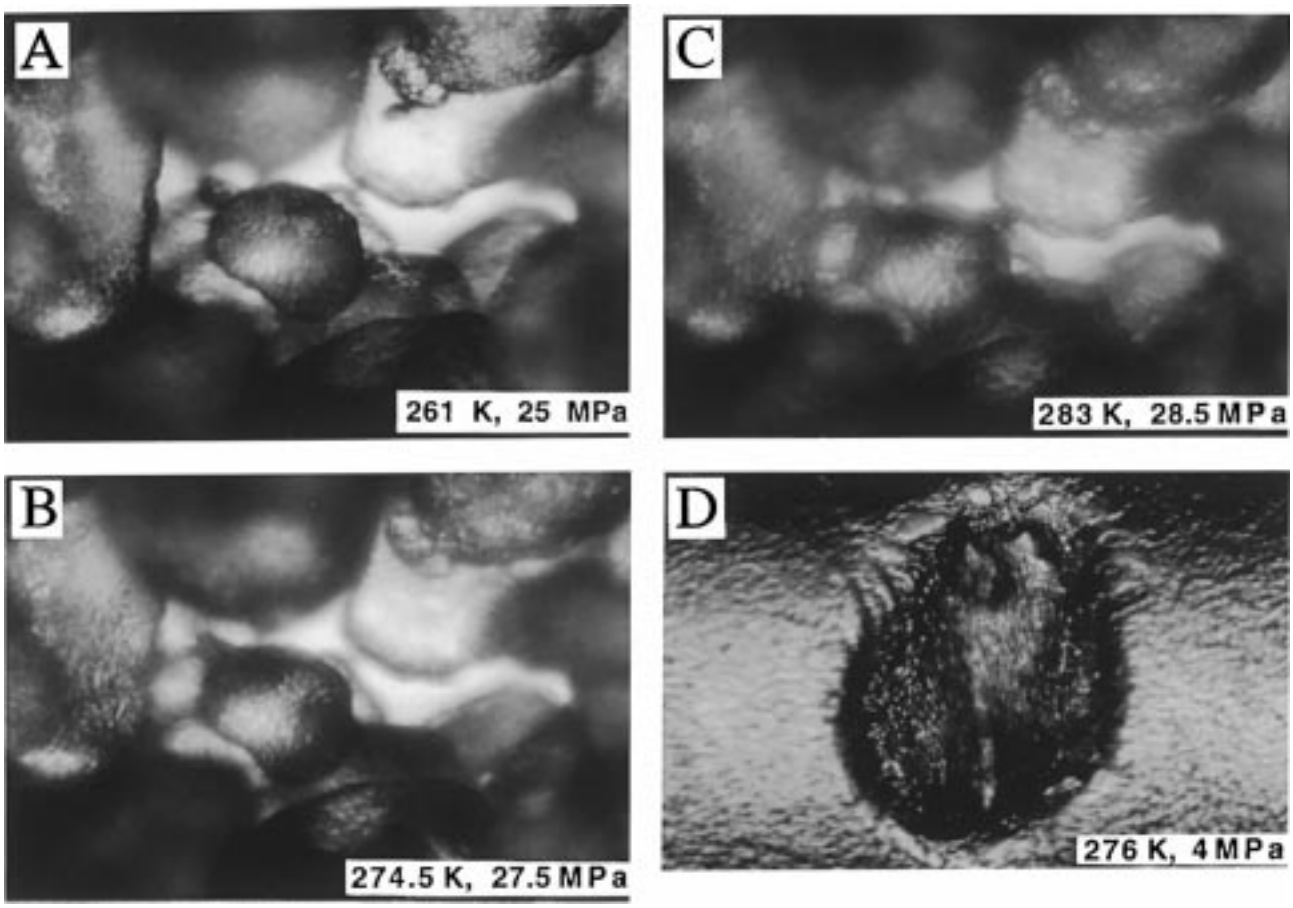

Figure 7. H_2O ice grains (180−250 μm grain size) and CH_4 gas reacting to form methane hydrate, shown in a series of photos for grains near the axis of the optical cell tube (see Figure 4, open circles, for $P-T$ locations.) Ice grains are initially smooth and glassy in appearance prior to exposure to a hydrate-forming gas, and retain this appearance throughout the 2-minute evacuation process.[17] (A) $T = 261$ K, $P_{CH_4} = 25$ MPa. After first exposure to pressurized CH_4 gas (or to CO_2, as described in text), the ice grains took on the mottled appearance shown here due to growth of a very thin surface layer of hydrate.[19] (B) $T = 274.5$ K, $P_{CH_4} = 27.5$ MPa; same grains as shown above. Grains have been warmed 3 °C above the H_2O liquidus for 0.5 h. (C) $T = 283$ K, $P_{CH_4} = 28.5$ MPa. Grains have been well above the H_2O liquidus for 1.5 h, but are still approximately 4 h from complete conversion to hydrate. Grains are approximately 60% reacted to hydrate, based on $P-T-$time relationships shown in Figure 4. Grains throughout the cell retained characteristic shapes and sizes, and there is no evidence for accumulation of liquid water despite lengthy exposure to warm T. Hydrate growth along the cell wall increasingly obscured viewing of grains located in the center of the cell,[20] but diagnostic grain shapes are still identifiable. (D) Induced melting of the superheated icy interior within a partially reacted grain after warming above the H_2O liquidus for 0.75 h at 274 to 276 K, and reducing P_{CH_4} from 27 to 4 MPa (see text). Grain became increasingly misshapen as liquid pooled within it, causing distortion of the hydrate shell. Water released from the grain rapidly formed hydrate, either along small fissures or as finely crystalline material surrounding the original grain.

eventually cracked or collapsed (Figure 7D) and eventually regrew with finely crystalline textures.[17] That this sample was maintained within the methane hydrate stability field and that no hydrate dissociation occurred was confirmed by observing (a) rapid hydrate crystallization accompanying liquid expulsion from the grain interiors, (b) the continual presence of hydrate along the optical cell wall, and (c) additional growth of methane hydrate crystals during the following 20 h at 275 ± 1 K. That all the crystalline material in the optical cell after 20 h was methane hydrate was confirmed by warming the sample to 277.5 K and observing its predicted decomposition to water plus gas when warmed through the dissociation curve. This full experimental sequence verified that hydrate-encrusted ice grains had persisted at elevated pressure to temperatures well above their ordinary melting point, and that their bulk melting is easily detectable and produces distinct melt textures that are in marked contrast to the stable shapes and sizes maintained by grains during standard fabrication procedures.

Discussion. The apparent suppression of macroscopic ice melting during methane hydrate synthesis raises several important questions; namely, why is full reaction achieved only after many hours at temperatures well above the H_2O ice melting point, and why is there no evidence for wholesale melting of unreacted seed ice during this time? Probably of greatest influence is the availability of fresh ice surfaces to nucleate hydrate formation. As previously discussed, for hydrate formation from either water or ice, the formation rate greatly diminishes once a surface layer of hydrate has formed, and vigorous shaking or stirring to crack the hydrate encasement and renew CH_4 access to ice/water surfaces has been routinely implemented to continue the formation process at appreciable rates.[6,15] Hwang and colleagues,[10] however, grew methane hydrate on disks of melting ice to measure hydrate growth rates at constant temperatures under static conditions. They observed two stages of methane hydrate formation, an initial "nucleation" period during which the formation rate increased with time, followed by a "growth" period,

during which the formation rate decayed with time until no more ice remained on the disks. Hydrate growth rates were shown not only to be determined by the rate of the supply of the hydrate-forming species to the growth surface but also by the rate of removal of the exothermic heat of formation from the forming surface.[8,21] They concluded that the onset of melting ice along exposed surfaces not only promoted hydrate formation by providing a "template" for the formation of hydrates, but moreover, provided a heat sink for absorbing the heat of formation during hydrate growth.

Our observations are in general accord with the results and conclusions discussed by Hwang et al.[10] We conclude that during our standard fabrication procedures, hydrate formation initially occurs in the ice subsolidus region, producing a thin plating of hydrate on the ice grain surfaces, and that subsequent hydrate formation occurs primarily by solid-state diffusion of the hydrate-forming species through the hydrate mantle to the ice core.[5,22] Although these diffusion and hydrate-forming processes are enhanced by the high P and T conditions of our fabrication methods, hydrate formation in the grain interior is likely rate-limited by the increasing diffusion distance between reactants as the hydrate barrier to the ice core grows and thickens (Figure 3), resulting in the long times needed for complete reaction. We hypothesize that reaction of a hydrate-forming species with incipient melting or "premelting"[23] at the hydrate−ice core interface may effectively inhibit the formation of an equilibrium solid−liquid water interface necessary for bulk melting, and can thus permit superheating of the remainder unreacted ice. A prominent superheating effect has been previously measured in gold-plated silver single crystals, and the results suggest that either a free external surface or internal defects or dislocations are critical for melting to take place at the normal "thermodynamic" melting point.[24] We note that our method of standard seed ice preparation produces grains with few internal grain boundaries, and additionally, the fine-grained ice is likely to anneal at the warm temperatures during synthesis, thus removing many of the internal defects for melt to nucleate on.

This model of hydrate growth from enhanced reactivity along superheated ice grain surfaces (at the ice core/hydrate mantle interface) is consistent with the $P-T-t$ records of our large-volume sample fabrications tests as well as with the optical cell observations of grains persisting to warm T at elevated P, with no appearance of free liquid, and with grain shapes and sizes remaining uniform with only limited outward growth.[25] The success of our method for full conversion of ice to hydrate, however, is apparently dependent on several aspects of our standard procedure that influence the availability and concentration of the hydrate-forming species at the growth front. The melt accumulation that accompanied the coarse-grained tests (1−2 mm) and the induced-melting optical cell test suggests that a prolonged superheating effect is at least partially dependent on those factors that influence diffusion rates, such as the surface area to volume ratio of the reacting grains, or the thickness of the developing hydrate barrier to the ice core. It is also possible that the larger seed ice fraction contains internal defects or dislocations that are not prevalent in the finer seed ice fraction, and that could serve as sites for melt nuclei.

Our premise for the induced melting experiment was that by reducing the rate of reaction of CH_4 with incipient melt at the hydrate−ice core interface, bulk melting could proceed. On the basis of our own experience and the work performed by Hwang et al.,[8,10] we speculated that reducing the driving potential for hydrate formation, by reducing the P overstep of the equilibrium line, should lower the rate of hydrate formation at the hydrate growth front and could thus serve as a method to induce melting of unreacted ice portions within grains. The success of the induced-melting test demonstrated not only that solid ice had been present within the reacting grains to melt but also demonstrated by corollary that excess P_{CH_4} is necessary to maintain a stable hydrate migration front to suppress bulk melting within the grain interiors at warm temperatures.

There remain numerous questions regarding this apparent superheating phenomenon which we do not yet fully understand and that will be the basis of future research. We note, however, that the parallel tests in the optical cell using both gaseous and liquid CO_2 as the hydrate-forming species confirm that the superheating effect can be reproduced in other gas-hydrate-forming systems under elevated conditions of P and T and that it is not a phenomenon unique to the CH_4-H_2O system.

Solid-State Deformation Testing and Results

Experimental Procedure. The strengths of seven methane hydrate specimens made by the above techniques were measured in constant-strain-rate tests in compression, at conditions ranging from $T = 140$ to 200 K, confining pressure (P_c) = 50−100 MPa, and strain rates ($\dot{\epsilon}$) = 3.5×10^{-4} to 10^{-6} s^{-1} (Table 1).

The testing apparatus is a 0.6 GPa gas deformation apparatus outfitted for cryogenic use,[26] in which N_2 or

(21) Hwang et al.[10] note that as hydrate formation is an exothermic process, the heat released by the phase change increases the temperature at the formation interface. This effect is greater for hydrate formation from liquid water than from ice since the heat of formation is partially absorbed by the melting ice.

(22) Conceptual models of hydrate growth by diffusion have been discussed previously by Makogan[9] and by Hwang et al.[10]

(23) "Premelting" of the ice grains (see review by: Dash, J.; Fu, H.; Wettlaufer, J. *Rep. Prog. Phys.* **1995**, *58*, 115, and references therein) may enhance reactivity and hydrate formation on ice grains along a disordered, liquidlike, surface film. Such subsolidus surface melt films are evidently sites of limited hydrate reaction, based on sample synthesis $P-T$ records and X-ray diffraction scans (see endnote 21 in ref 5). (See also discussion of interface phase transitions in: Sutton, A.; Balluffi, R. *Interfaces in Crystalline Materials*; Clarendon Press: Oxford, U.K., 1995; Chapter 6).

(24) Daeges, J.; Gleiter, H.; Perepezko, J. *Phys. Lett.* **1986**, *119A*, 79. See also: Phillpot, S.; Lutsko, J.; Wolf, D.; Yip, S. *Phys. Rev. B* **1989**, *40*(5), 283−2840; and Phillpot, S.; Yip, S.; Wolf, D. *Comput. Phys.* **1989**, *3*, 20−31, for further discussion of results.

(25) It remains unclear how ΔV of ice → hydrate conversion[11] is accommodated during reaction. The large ΔV (0.16) should produce a P gradient within composite ice/hydrate grains at the hydrate growth front, yet we observe no evidence for external cracking of the hydrate encasement nor a substantial increase of fully-reacted grain diameters. We speculate that the volumetric differences may be accommodated by a diffusive flux of H_2O within the hydrate mantle, removal of some hydrate material through sublimation,[20] or brittle/ductile behavior of the hydrate mantle that is below our resolution levels.

(26) Heard, H.; Durham, W.; Boro, C.; Kirby, S. In *The Brittle-Ductile Transition in Rocks*; Geophysical Monograph 56; Duba et al., A. G., Eds.; American Geophysical Union: Washington, DC, 1990; pp 225−228.

Table 1. Mechanical Test Conditions and Results

run no.	step	T (K)	P_c (MPa)	$\dot{\epsilon}$ (s^{-1})	ϵ_t	σ_y (MPa)	σ_{ss} (MPa)	comments
281	1	160	50	3.5×10^{-4}	0.125		>85	strain hardening
	2	160	50	3.5×10^{-6}	0.150		60	strain hardening
	3	160	50	3.5×10^{-4}	0.160	100		brittle failure; ≈25% H_2O ice[b]
282	1	140	50	3.5×10^{-6}		71		failure, multiple events
	2	140	50	3.5×10^{-4}	0.160	94		failure, multiple events; ≈25% ice[b]
366	1	168	100					pressurization and compaction only[c]
367	1	185	100	3.5×10^{-5}	0.138		71	strain hardening at 10^{-5} step
	2	185	100	3.5×10^{-4}	0.215	96	90	≈30% ice postdeformation
368	1	168	100	3.5×10^{-5}	0.185		102	strain hardening; 25% ice[b]
369	1	168	100	3.5×10^{-5}	0.16		100	identical run as 368[d] no evolved CH_4 gas
370	1	200	100	3.5×10^{-5}	0.120		62	strain hardening at 10^{-5} no evolved gas[d]
	2	200	100	3.5×10^{-4}	0.230	85	80	≈30% ice postdeformation

[a] P_c is confining pressure gas medium; ϵ_t is total strain; σ_y is yield strength; σ_{ss} is steady-state strength. [b] Postdeformation, determined by X-ray diffraction. [c] Samples 367, 368, 369, and 370 all underwent identical pressurization and compaction as 366 prior to testing. [d] Runs 369 and 370 had a gas collection system attached throughout testing to detect evolved CH_4 gas (see Figure 8).

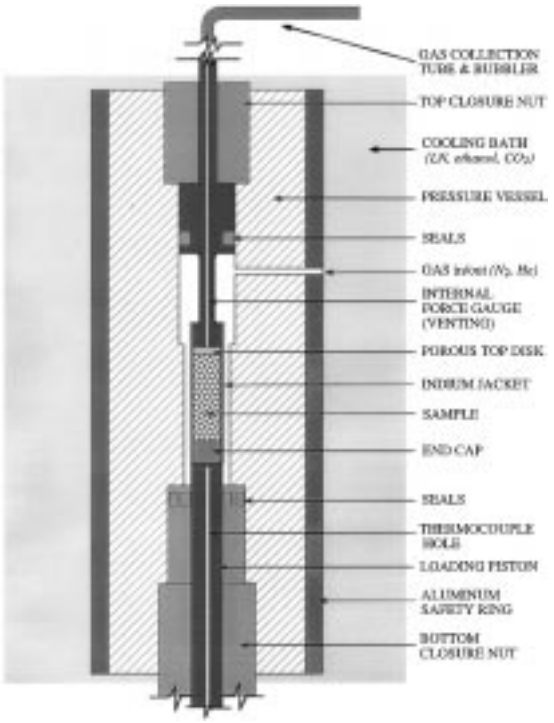

Figure 8. Schematic of triaxial gas deformation apparatus for methane hydrate testing at cryogenic temperatures. The indium-jacketed sample within the cylindrical pressure vessel is under pressure provided by a confining medium gas (N_2 or He). A sliding piston moves through dynamic seals from below to impose constant axial shortening. Samples are mounted on to a "venting" internal force gauge permitting sample communication with room pressure and allowing initial hydrostatic pressurization to eliminate residual porosity prior to deformation. The gas collection system (shown at top) was attached during several tests to monitor possible loss of methane gas during deformation (see text).

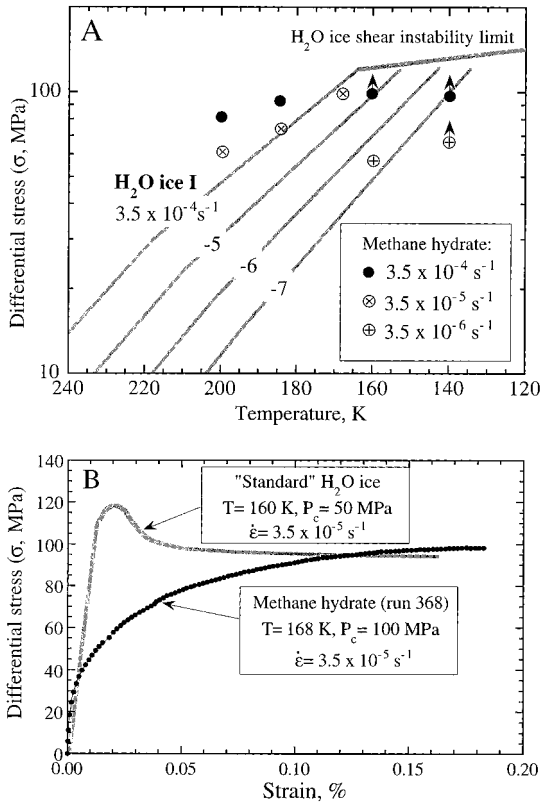

Figure 9. (A) Strength measurements of methane hydrate show that it has measurably different strength than polycrystalline H_2O ice. Ice flow law constants are from ref 27. Methane hydrate data points with arrows indicate faulting behavior. (B) Stress−strain curves of deformed methane hydrate (run 368) compared to polycrystalline H_2O ice. While the strengths of the two compounds are comparable, methane hydrate undergoes systematic strain hardening to an extreme degree (over 18% strain) while H_2O ice typically displays an ultimate yield strength followed by relaxation to steady-state behavior.

He gas provides the confining pressure (P_c) medium (Figure 8). The thin, soft, indium jackets in which the samples were grown serve to encapsulate them during testing to exclude the P_c medium, and provide the additional benefit of superbly replicating the outer surface of the deformed sample and thus enabling subsequent microstructural study at room conditions. Sample interiors were vented to room conditions by means of small-diameter tubing to allow initial compaction to eliminate porosity. The pressurized column within the apparatus consists of an internal force gauge, the jacketed sample, and a moving piston that compresses the sample axially against the internal force gauge at a fixed selected displacement rate ($\dot{u}$). Elastic

(27) Durham, W.; Kirby, S.; Stern, L. *J. Geophys. Res.* **1997**, *102* (E7), 16, 293−16, 302.

(28) We thank Tim Collett, Tom Lorenson, Joe Hightower, and one anonymous referee for providing helpful reviews of the manuscript. This work was supported under NASA order W-18,927, and was performed in part under the auspices of the USGS and in part by the U.S. DOE by the Lawrence Livermore National Laboratory under contract W-7405-ENG-48.

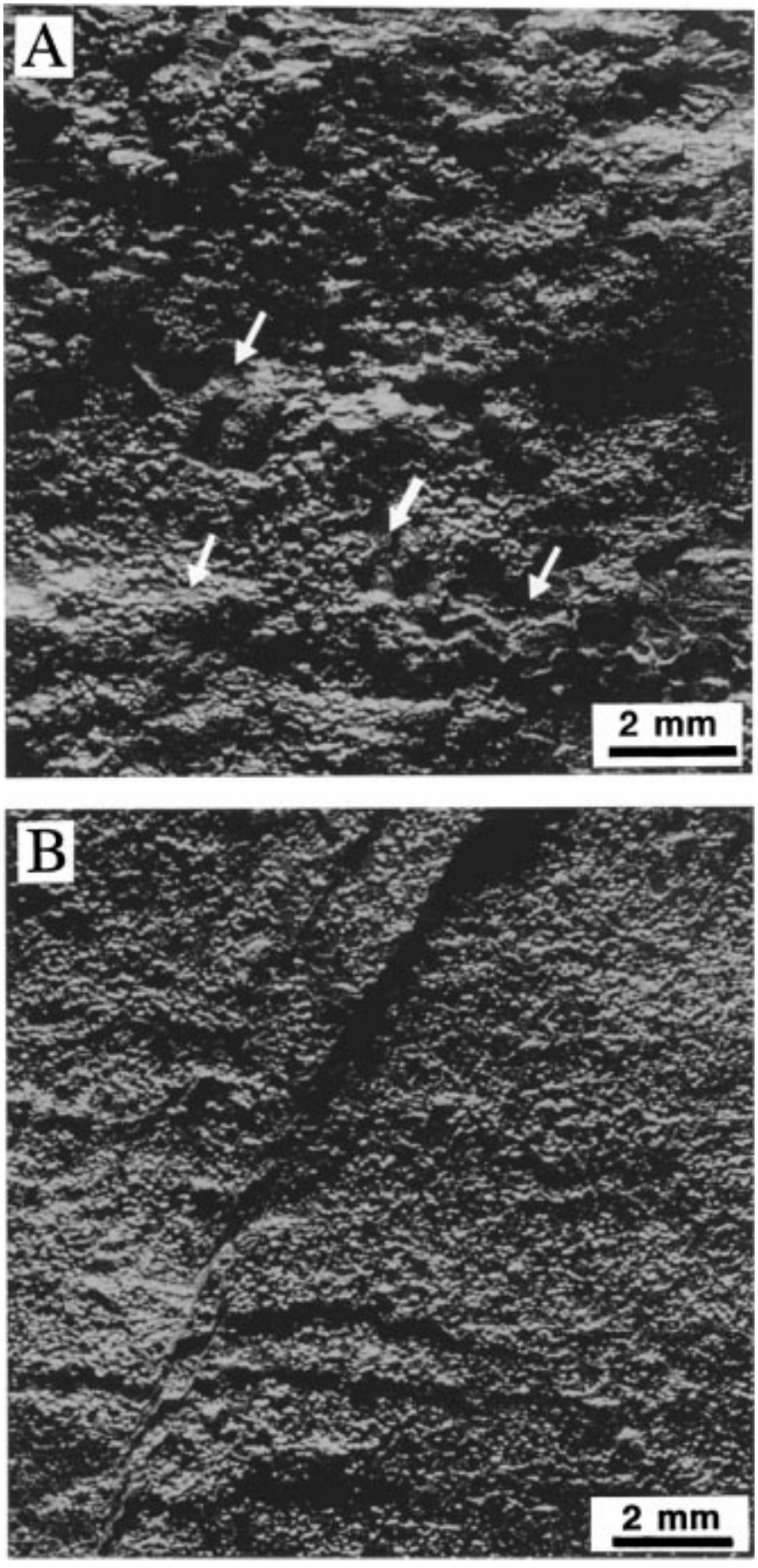

Figure 10. Indium jacket replicas of the surfaces of samples deformed within the ductile (A) and brittle (B) regimes. Compression direction is oriented vertically in both photographs. (A) Sample 367, deformed at 185 K, 100 MPa, and taken to 21% strain (Table 1). Oblique illumination highlights the surface topology and shows deformed grains standing in relief. Some of the plastically deformed hydrate grains show pronounced elongation in the plane perpendicular to the direction of compression, presumably produced by dislocation creep. Many of the grains have grown significantly from their original size, likely by stress-induced coalescence of impinging grains within the compression plane. Fine-grained patches (such as those marked by arrows) are believed to be regions of precipitated ice (see text). (B) Sample 282, tested at 140 K and 50 MPa, that was taken to 16% strain and faulted during several events (Table 1). The individual grains and the fault trace on the jacket stand out in relief. Grain shapes and sizes in the cold, brittle-regime samples remain equant and uniform at $\sim 250 \pm 50$ μm.

distortion of the force gauge is measured outside the vessel and changes only with P_c and with the differential load that the piston exerts on the sample. In these experiments, differential force (F) and piston displacement (u) are recorded, corrected for changes from initial cross-sectional area and length (A_0, L_0) to instantaneous values (A, L), and converted to differential stress (σ), axial shortening strain (ϵ), and strain rate ($\dot{\epsilon}$) by the relationships

$$\epsilon = u/L_0; \quad \dot{\epsilon} = \dot{u}/L; \quad A \cdot L = A_0 \cdot L_0; \quad \sigma = F/A$$

The force−time record (which we convert to stress−strain, as in Figure 9B) usually reveals a transient response followed by a strength that ceases evolving with time, when various processes of work hardening and recovery have reached a steady-state condition.

Samples were subjected to a hydrostatic pressurization and compaction sequence at 170 K, prior to deformation. During this procedure, P_c was slowly "stepped" up to 100 MPa in increments of roughly 20 MPa. Following each P step, the piston was advanced to touch and square the bottom of the sample, and then advanced just sufficiently to lightly compress the sample in order to compact it with minimal plastic deformation. Five of the samples were compacted using the internal vent line to eliminate the pore-space gas, and two of the samples were compacted without the venting capability. One sample (run 366, Table 1) was examined after compaction in the undeformed state. Volumetric measurements showed that virtually all porosity was eliminated and that a cylindrical shape was largely maintained with only minor distortion of the sample. X-ray analysis showed evidence of a small fraction of H_2O ice in the sample ($\sim 7 \pm 3\%$), likely due to a disproportionation of hydrate as increasing P effects a stoichiometric change from $CH_4 \cdot 6.1H_2O$ to $CH_4 \cdot 5.8H_2O$.[12]

Deformation Test Results. Methane hydrate samples displayed measurably different steady-state strengths than H_2O ice, and the results are summarized in Figure 9A. Moreover, the characteristics of transient deformation are markedly different. A typical stress−strain curve for methane hydrate is shown in Figure 9B; whereas H_2O ice ordinarily exhibits a strength maximum before leveling off to steady flow stress, usually within the first 5−10% of strain, methane hydrate exhibits monotonic work hardening (or strain hardening) that continues over more than 15% strain. This hardening effect persists to an extreme degree not only relative to other ices but to most metals and ceramics at high homologous temperatures as well.

Comparison of pre- and postdeformation X-ray diffraction analyses shows that samples underwent further structural changes while deforming within the nominal hydrate stability field. All deformed samples showed a significant volume fraction of ice in their final X-ray patterns ($25 \pm 10\%$, Figure 5B) compared with virtually no ice in their pretest X-ray patterns (<3%, Figure 5A), and also showed larger fractions of ice than detected in the pressurized-only sample (run 366). It is possible, however, that either heterogeneous ice precipitation or deformation-enhanced textural and grain size changes in the precipitated ice increased the apparent ice peak intensities (Figure 10). No peaks were observed in postdeformation X-ray patterns to indicate growth of any other new phase besides ice and structure I hydrate. We note that the two nonvented samples (281 and 282, Table 1), showed equally large fractions of ice in their postdeformation X-ray patterns as the vented samples. After first detecting this apparent solid-state disproportionation of the hydrate, a gas collection system was attached to the vent line for two of the runs to observe and collect possible CH_4 gas evolving during deformation (Figure 8). The only gas that appeared from the vent, however, was that squeezed from the pores during initial pressurization before deformation. No gas evolved from the system during any portion of deformation testing or subsequent unloading. While collapse of the hydrate structure could occur if as-molded material were strongly nonstoichiometric and contained significant lattice vacancies, this is unlikely as we measured nearly full uptake of CH_4 gas into the as-molded material. Double occupancy in lattice cages also seems unlikely as a possible explanation due to spatial considerations. We therefore conclude that at the deformation conditions of this study, methane hydrate appears to undergo a form of stress-enhanced exsolution and/or precipitation process within its nominal stability field. Precipitating H_2O ice may possibly be causing a dispersion hardening process during hydrate deformation, a process that is targeted for further study.

Summary

Methane hydrate displays exceptional characteristics that merit further investigation into the nature and behavior of this important compound. In the course of establishing optimal growth parameters for synthesizing hydrate samples suitable for rheological testing, we demonstrated that under conditions favorable to hydrate formation and at elevated pressure, the rate of H_2O ice melting can be suppressed to allow short-lived superheating of ice to temperatures well above its ordinary melting point. Deformation tests showed that not only does methane hydrate have a measurably different rheology than H_2O ice but that it also undergoes extensive work hardening accompanied by a process of solid-state disproportionation during deformation at conditions well within its equilibrium stability field. Such unexpected consequences of methane hydrate formation and deformation may affect the physical, mechanical, and geochemical properties of hydrate-bearing sediments in ways not previously appreciated. In particular, hydrate instability under nonhydrostatic stress may affect environments such as those underlying continental shelves or in associated accretionary prisms prone to regional tectonic influences, where the presence of hydrates influences the strength, stability, porosity, and permeability of hydrate-cemented sediments.

EF970167M